2002-01-2729

Parameterization and Transient Validation of a Variable Geometry Turbocharger for Mean-Value Modeling at Low and Medium Speed-Load Points

Merten Jung, Richard G. Ford, Keith Glover and Nick Collings
University of Cambridge

Urs Christen and Michael J. Watts
Ford Motor Company

ABSTRACT

The parameterization of variable geometry turbochargers for mean-value modeling is typically based on compressor and turbine flow and efficiency maps provided by the supplier. At low turbocharger speeds, and hence low airflows, the heat exchange via the turbocharger housing affects the temperature-based measurements of the efficiencies. Therefore, the low-speed operating regime of the turbocharger is excluded from the supplied maps and mean-value models mainly rely on extrapolation into this region, which is regularly met in emission drive cycles, and hence of significance.

This paper presents experimental data from a 2.0-liter turbocharged common-rail diesel engine. While the flow maps extend from the high-speed region in a natural way, the efficiency maps are severely affected by the heat transfer effect. It is argued that this effect should be included in the mean-value model. A physics-based parameterization is suggested for the turbine efficiency, which poses the biggest problems in turbocharger modeling. This new model structure is then validated with transient engine data.

1 INTRODUCTION

Modern diesel engines are typically equipped with variable geometry turbochargers (VGT) and exhaust gas recirculation (EGR), which both introduce feedback loops from the exhaust to the intake manifold. This leads to a substantial increase in calibration effort. Model-based control aims at reducing this effort but relies on the underlying model. While crank-angle resolution models are still far too complex for the purpose of control, mean-value modeling has been given a lot of attention in the past. For the air path, the crucial part of the overall model is the turbocharger. The modeling of this highly nonlinear device relies typically on performance maps provided by the supplier. However, due to heat transfer effects and flow measurement problems [9], these maps are only provided for medium and higher turbocharger speeds (i.e. >90,000 rpm for the VGT under investigation in this paper), which are only reached in the higher speed-load range of the engine. In the low and medium speed-load range, which is important for emission drive cycles for example and where turbocharger speeds are as low as 10,000 rpm, most models simply rely on the extrapolation of the mapped data [6,7,9,10]. In [1], some lower speed data from a static burner test-bench are included and parameterized.

Due to the poor extrapolation capabilities of regressions in general, the parameterizations of the turbocharger maps are typically physics-based. A good overview of different parameterization methods can be found in [9]. The authors particularly address the extrapolation capabilities to the low speed region, observing some difficulties with neural networks. The elimination of these problems is reported in [3]. The authors successfully apply an artificial neural network to VGT modeling. Neural networks can be very helpful for simulation studies; however, they cannot readily be used for standard model-based control design methodologies.

In this paper, the turbocharger maps at low and medium speed-load points are obtained experimentally from a 2.0-liter common-rail diesel engine equipped with a VGT and a turbocharger speed sensor. The data are used to assess the accuracy of the extrapolation of the supplied maps to lower turbocharger speeds. It turns out that while the flow maps extend naturally to this region, the efficiency maps are significantly affected by the heat transfer from the turbine to the compressor side via the turbocharger housing at low flow rates. The heat transfer decreases the measured temperature before the turbine and increases the post compressor temperature, which renders the compressor efficiency artificially low and the turbine efficiency artificially high. This phenomenon justifies the fact that they are excluded from provided turbocharger maps. This effect is also observed and

implicitly parameterized in [1] using low turbocharger speed data obtained from a static burner test-bench, but only for the compressor side.

In mean-value models, the efficiencies are used to calculate the turbocharger speed (via a power balance between turbine and compressor) and the temperatures post compressor and post turbine. If the heat transfer effect is included in both compressor and turbine efficiency, the turbocharger speed can be predicted correctly. In order to distinguish between aerodynamic efficiency and the efficiency including heat transfer effects, the latter will subsequently be called *pseudo-efficiency*. With respect to the temperatures, these pseudo-efficiencies are actually needed to get the correct values.

While the heat transfer effect on the compressor efficiency does not pose severe problems either to measurement or to parameterization, the turbine efficiency is different. At pressure ratios close to one across the turbine (which occur at the lower and medium speeds this paper is focused on), the measured efficiency based on temperatures becomes very sensitive to the pressure fluctuations of the pulsating flow. Moreover, it is difficult to obtain representative temperature readings, because a closed-coupled oxidation catalyst with its high thermal inertia makes it impractical to wait for the system to assume equilibrium at each new operating point. At some points, an exothermal reaction in the catalyst rendered the post turbine temperature even higher than pre turbine leading to negative efficiencies. As will be shown in Section 4.4**,** this problem can be overcome by calculating the turbine efficiency from the compressor efficiency in steady-state.

The second problem with respect to the turbine efficiency is its parameterization. This is already critical without including the effect of heat transfer, since the efficiency depends on the turbocharger speed, the pressure ratio across the turbine, and the guide vane position. The way forward suggested in this paper in Section 5.4 is to separate the heat transfer effect and to parameterize the efficiency map in a conventional way using the blade speed ratio [4]. The pseudo-efficiency is then obtained by adding the efficiency due to the heat transfer by modeling the turbocharger housing as a heat exchanger with flow dependent cooling effectiveness.

The next section gives a brief introduction to the modeling of turbochargers using compressor and turbine flow and efficiency maps and how they are embedded in an overall engine model. Section 3 presents the experimentally obtained maps from a 2.0-liter common-rail diesel engine equipped with VGT and EGR. Section 4 describes the parameterization of these maps with focus on the turbine efficiency map. Finally, the transient performance of the VGT model (which is parameterized based on the experimental steady-state data) embedded in the overall engine model is compared to engine data for different transient excitations. Note that for subsequent control design, the transient performance is more important than the steady-state accuracy, because any reasonable controller will take care of steady-state errors. A good transient model is required for optimal controller performance.

2 EXPERIMENTAL SETUP

The engine setup under investigation is depicted in Figure 1. The four cylinder 2.0-liter common-rail diesel engine (130 bhp @ 3800 rpm, 325 Nm @ 1800 rpm) is equipped with a variable geometry turbocharger and exhaust gas recirculation. The recirculated exhaust gas is cooled down in the EGR cooler and its mass flow is controlled via the EGR valve. Both the EGR valve and the VGT are pneumatically actuated and fitted with position sensors. An intercooler reduces the temperature of the compressed air coming from the compressor.

In addition to the standard production type sensors, e.g. for mass air flow (MAF) and manifold absolute pressure (MAP), the engine is equipped with various temperature and pressure sensors as well as with a turbocharger speed and inline shaft torque sensor. The temperature sensors are standard thermocouples (Type K, 1.5 mm, 0.3 s response time, not radiation shielded). The steady-state temperature values are obtained by low-passing the measurements. Due to the faster response time of the pressure sensors and the MAF sensor, these measurements are more fluctuating in the pulsating flow of the engine. In order to reduce measurement errors due to improper sampling, these signals are sampled each crank degree and then averaged over each engine cycle before low passing them.

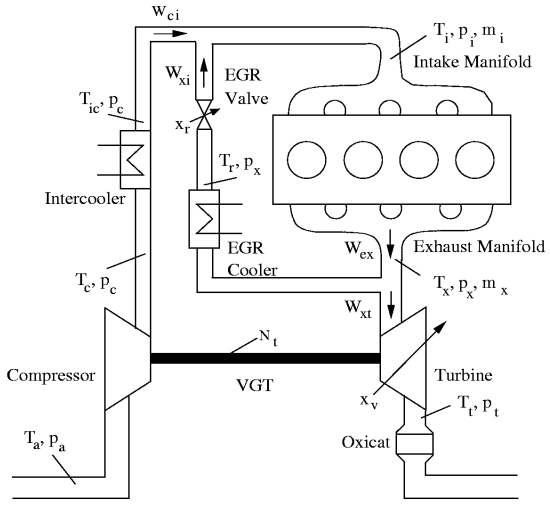

Figure 1: Engine setup.

The ECU is bypassed via a CAN interface as described in [12]. This allows access to internal variables of the

ECU and control over the engine via a dSPACE rapid prototyping system, which is also used for the data acquisition.

3 MEAN-VALUE ENGINE MODELING

The engine model used in this paper was developed by Christen et al. [2]. It is event-based rather than time-based which was shown to be beneficial for applications involving flows [11], since the flow-related parameters are less varying in the event domain. The corresponding time-based model was established in [4]. In order to avoid confusion, the equations stated in this paper are all time-based, but the conversion to events is straightforward and can be found e.g. in [2].

The turbocharger submodel in [2] uses a parameterization of the provided flow and efficiency maps and extrapolates them into the low speed region. In this paper, experimental data is obtained for the low-speed region, thus making extrapolation unnecessary.

The next section familiarizes the reader with the basic equations of the turbocharger modeling using provided flow and efficiency maps. Section 3.2 then briefly describes the other subsystems of the engine model, which are joined together to form the overall model presented in Section 3.3.

3.1 TURBOCHARGER

The turbocharger consists of a turbine driven by the exhaust gas and connected via a common shaft to the compressor, which compresses the air in the intake. The rotational speed of the turbocharger shaft can be derived as a power balance between the turbine and the compressor side

$$\dot{N}_t = \left(\frac{60}{2\pi}\right)^2 \frac{P_t - P_c}{J_t N_t} \tag{1}$$

where the turbocharger speed is measured in rpm and J_t is the inertia of the turbocharger. Subsequently, the expressions for the compressor and turbine power are derived separately.

3.1.1 Compressor

Assuming that the compression process is isentropic, the following relation between the temperature and pressure at the inlet (T_a, p_a) and at the outlet ($T_{c,is}$, p_c) of the compressor can be derived

$$\left(\frac{T_{c,is}}{T_a}\right) = \left(\frac{p_c}{p_a}\right)^{\frac{\gamma-1}{\gamma}} \tag{2}$$

However, due to enthalpy losses across the compressor (e.g. incidence and friction losses), the compression process is not isentropic in reality. Therefore, the compressor isentropic efficiency is introduced which relates the theoretical temperature rise (leading to $T_{c,is}$) to the actual (resulting in T_c)

$$\eta_c = \frac{T_{c,is} - T_a}{T_c - T_a} \tag{3}$$

Substituting this into (2) yields the expression for the temperature downstream of the compressor:

$$T_c = T_a + \frac{1}{\eta_c} T_a \left(\left(\frac{p_c}{p_a}\right)^{\frac{\gamma-1}{\gamma}} - 1 \right) \tag{4}$$

In order to derive an equation for the compressor power, the first law of thermodynamics is applied which states that (neglecting heat losses) the compressor power is related to the mass flow through the compressor W_{ci} and the total change of enthalpy by

$$P_c = W_{ci}(h_c - h_a) = W_{ci} c_p (T_c - T_a) \tag{5}$$

where the second equality assumes constant specific heats. Applying (4) to this equation finally gives the expression for the compressor power

$$P_c = W_{ci} c_p T_a \frac{1}{\eta_c} \left(\left(\frac{p_c}{p_a}\right)^{\frac{\gamma-1}{\gamma}} - 1 \right) \tag{6}$$

In order to calculate the compressor power in (5), the compressor efficiency and mass flow have to be known. These variables are highly nonlinear functions of the pressure ratio across the compressor and the turbocharger shaft speed. As mentioned in the introduction, these maps are provided by the supplier for medium and high turbocharger speed obtained from steady-flow test benches. Section 4 presents these maps obtained under the pulsating flow conditions in the engine for low and medium turbocharger speeds.

3.1.2 Turbine

The expressions for the turbine outlet temperature and power can be derived similarly to the compressor outlet temperature (4) and power (6) yielding

$$T_t = T_x - \eta_t T_x \left(1 - \left(\frac{p_t}{p_x}\right)^{\frac{\gamma-1}{\gamma}} \right) \tag{7}$$

and

$$P_t = W_{xt} c_p T_x \eta_t \left(1 - \left(\frac{p_t}{p_x} \right)^{\frac{\gamma-1}{\gamma}} \right) \tag{8}$$

Again, the turbine flow W_{xt} and isentropic efficiency η_t are mapped versus the pressure ratio across the turbine and the turbocharger shaft speed. However, these variables also depend on the position of the variable guide vanes, which replace the conventional waste gate to avoid overspeeding at high engine loads without sacrificing the low load performance. For the turbine flow map, the dependence on the turbocharger speed can be neglected, however, this is not the case for the turbine efficiency. Hence, the turbine efficiency map is four dimensional (as opposed to three dimensions for the other maps), rendering it very difficult to parameterize. Including the effect of heat transfer complicates the parameterization even more. However, in Section 5, a new physics-based method to overcome this problem is suggested.

In order to simulate the pressure ratio across the turbine, the exhaust backpressure needs to be modeled. It is fitted as a quadratic polynomial in the volumetric flow $W_{xt}RT_t/p_t$. This equation forms an algebraic loop with the turbine equations, and hence, fast dynamics have to be included in the implementation to break it.

3.2 OTHER SUBSYSTEMS

3.2.1 Engine Block

From Newtonian Mechanics, the crankshaft dynamics can be derived as

$$\dot{N} = \frac{60}{2\pi} \frac{T_b - T_l}{J_e + J_{dr}} \tag{9}$$

where J_e and J_{dr} are the engine and driveline inertias, respectively. T_l is the load torque and the brake torque $T_b=T_{ind}-T_f$ is the difference between the indicated torque (obtained from cylinder pressure data and approximately proportional to the injected fuel mass per stroke) and the friction torque (identified from engine data and fitted as a quadratic polynomial in engine speed). The mass flow rate from the intake manifold into the cylinders is determined by the speed density equation

$$W_{ie} = \eta_v \frac{m_i}{V_i} \frac{N}{60} \frac{V_d}{2} \tag{10}$$

with the volumetric efficiency η_v (fitted as polynomial in engine speed and intake manifold pressure) and the total displacement volume V_d.

For the modeling of the conditions in the exhaust manifold in the next section, the temperature of the mass flow from the cylinder into the exhaust manifold has to be modeled. This is achieved by a fitted polynomial in fuel flow, airflow into the cylinders, and engine speed.

3.2.2 Manifolds

The intake and exhaust manifolds are modeled as open thermodynamic systems, where the mass of gas can increase or decrease with time (so-called *filling and emptying model*). The two governing equations for such systems are the *Conservation of Mass* and the *Conservation of Energy*. Neglecting heat losses through the manifold walls and assuming an ideal gas with constant specific heats, the differential equations for the manifold pressures are derived as

$$\begin{aligned} \dot{p}_i &= \frac{\gamma R}{V_i} \left(T_{ic} W_{ci} + T_r W_{xi} - T_i W_{ie} \right) \\ \dot{p}_x &= \frac{\gamma R}{V_x} \left(T_e W_{ex} - T_x \left(W_{xi} + W_{xt} \right) \right) \end{aligned} \tag{11}$$

and for the accumulated masses in the manifolds as

$$\begin{aligned} \dot{m}_i &= W_{ci} + W_{xi} - W_{ie} \\ \dot{m}_x &= W_{ex} - W_{xi} - W_{xt} \end{aligned} \tag{12}$$

The manifold temperatures cannot be assumed to be constant and are calculated from the ideal gas law as

$$\begin{aligned} T_i &= \frac{V_i}{R m_i} p_i \\ T_x &= \frac{V_x}{R m_x} p_x \end{aligned} \tag{13}$$

3.2.3 Exhaust Gas Recirculation

Under the assumption that no mass is accumulated in the EGR system it can be modeled with static equations rather than with differential equations. The flow through the EGR valve is determined by the standard orifice flow equation [5]

$$W_{xi} = \frac{A_r(x_r) p_x}{\sqrt{RT_x}} \sqrt{\frac{2\gamma}{\gamma - 1} \left[p_r^{\,2/\gamma} - p_r^{\,(\gamma+1)/\gamma} \right]} \tag{14}$$

with the pressure ratio

$$p_r = \max \left(\frac{p_i}{p_x}, \left(\frac{2}{\gamma + 1} \right)^{\frac{\gamma}{\gamma-1}} \right) \tag{15}$$

in order to describe subsonic as well as choked EGR flow. The effective area A_r is identified as a quadratic polynomial of the normalized valve lift x_r.

3.2.4 EGR- and Intercooler

The downstream temperatures of both the EGR- and the intercooler are calculated using the heat exchanger effectiveness and the appropriate upstream and coolant temperatures

$$T_{down} = \eta_{h.e.} T_{cool} + (1 - \eta_{h.e.}) T_{up} \tag{16}$$

Pressure drops across the coolers are neglected.

3.3 OVERALL DIESEL ENGINE MODEL

The models of the subsystems from the previous sections can be connected to an overall model consisting of coupled first-order nonlinear differential equations. The model comprises eight states, i.e. the intake and exhaust manifold pressures and accumulated masses, the engine as well as the turbocharger speed, the compressor mass flow (introduced in (22) below), and one state to break an algebraic loop as mentioned at the end of Section 3.1.2. The inputs to the system are the injected fuel mass, the load torque, and the normalized EGR and VGT actuator positions. For numerical simulations, the model is implemented in Simulink.

The main assumptions made to derive this model are:

- Ideal gases with constant specific heats
- No heat loss through manifold walls
- No pressure drop across the EGR- and intercooler and constant heat exchanger effectiveness
- No accumulated mass in the EGR system

These assumptions show that the model is of limited complexity only, which is justified by its purpose for control design. Transport and time delays, which are actually important for control design, have not been incorporated at this stage and further investigation is necessary but does not lie within the scope of this paper. Due to low gas velocities, the differences between static and dynamic pressures and temperatures are neglected.

Note that the assumption of no heat loss through the exhaust manifold is not exactly true. The temperature rise in the cylinder has been identified from steady-state data of the exhaust temperature, thereby implicitly including heat losses. This appears to be reasonable for the conditions encountered in the exhaust manifold.

4 EXPERIMENTAL TURBOCHARGER MAPS

In order to avoid the dependence of the maps on the temperature and pressure upstream of the compressor and turbine, the following normalized (corrected) quantities are used

$$\Phi_1 = W_1 \frac{\sqrt{T_{1,up} / T_{ref}}}{p_{1,up} / p_{ref}} \tag{17}$$

and

$$\widetilde{N}_{t1} = N_t \sqrt{T_{ref} / T_{1,up}} \tag{18}$$

where the subscript *1* refers to the compressor or turbine depending on which map is considered. The reference temperature and pressure are chosen as 298 K and 101.3 kPa.

4.1 COMPRESSOR FLOW

4.1.1 Measurement

The compressor flow is measured with a production type mass airflow (MAF) sensor. Although its accuracy is typically only 7 %, it has the advantage of covering the whole engine operating regime. Alternatively, the flow can be measured by determining the differential pressure across an orifice as the supplier does it on the test bench. However, for good accuracy especially at low flows, a vast set of orifice plates of appropriate sizes has to be used which has been considered impractical for this application. The post compressor pressure is obtained from a pressure sensor in the intake manifold while the upstream pressure is assumed to be constant and equal to ambient conditions. Note that there is a flow dependent pressure drop across the air filter, which can be as high as 3 kPa at full load. In the operating regime considered here, the maximum pressure drop was 1 kPa. However, this inlet depression effect is not included in the mean-value model, and hence the pressure ratio should be measured based on ambient upstream pressure as well, thereby implicitly including this effect.

The upstream temperature is also set constant to ambient in the mean-value model. However, on the engine it increases depending on the operating point by up to 10 K, thereby having a significant effect on the compressor maps, especially on the compressor efficiency in Figure 3. As for the pre compressor pressure, rather than modeling this effect it is implicitly included in the compressor maps by using ambient upstream conditions in the normalization of the data and the calculation of the compressor efficiency. This has the advantage of parameterizing these effects dependent on turbocharger speed and pressure ratio without additional modeling effort. The disadvantage is that the experimental data in Figure 2 and 3 are not directly comparable to the provided data from the manufacturer who uses the measured upstream conditions. In order to gain confidence in the accuracy of the measurements, the compressor flow and efficiency have been obtained experimentally using the measured upstream conditions, which coincided with the provided data quite nicely.

4.1.2 Experimental Results

The experimental data are plotted in Figure 2. The red crosses denote the data obtained from the engine for normalized turbocharger speeds in the range from 20,000 to 110,000 rpm, while the green circles represent the data supplied by the manufacturer. As mentioned earlier, the latter are only available for speeds larger than 90,000 rpm. The black solid lines correspond to the curve fit, which is described in Section 5.

For a fixed turbo speed, the speed lines are very flat at low flows (surge region, inability to deliver a steady flow against an increasing post compressor pressure until backflow occurs, which can seriously damage the compressor) and become very steep for high flows (choke region, the air velocity reaches the speed of sound and no more flow can be delivered even if the post compressor pressure decreases further). The steady-state operating regime of the engine lies between the surge and choke region as can be seen from the experimental data.

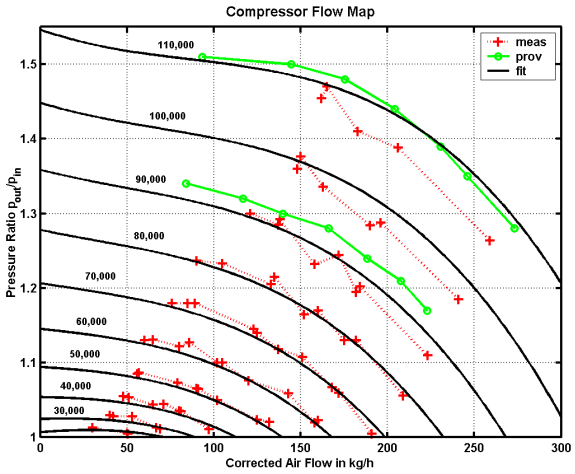

Figure 2: Compressor flow map: Measured, provided, and fitted data for different turbocharger speeds. The provided data in this and the following figures are plotted with permission from Honeywell Garrett. Note that the provided and measured data are not directly comparable as discussed in Section 4.1.1; the provided data are plotted for qualitative comparison only.

4.1.3 Discussion

The experimental data in Figure 2 confirm what would be expected as a reasonable extrapolation of the data provided at higher turbocharger speeds. The slight mismatch between the experimental and supplied data at turbocharger speeds of 90,000 and 110,000 rpm, respectively, can be explained by the assumption of constant pressure and temperature at the compressor inlet as mentioned in Section 4.1.1. Using the measured upstream conditions the data coincide very well. It should again be pointed out that in the mean-value model, ambient conditions at the compressor inlet are assumed, and hence, the measured data should be used for parameterization.

4.2 COMPRESSOR EFFICIENCY

4.2.1 Measurement

The compressor efficiency cannot be measured directly and has to be calculated based on the pressure and temperature ratios across the compressor. Rearranging (4) yields

$$\eta_c = \frac{\left(\frac{p_c}{p_a}\right)^{\frac{\gamma-1}{\gamma}} - 1}{\frac{T_c}{T_a} - 1} \tag{19}$$

which becomes sensitive to measurement errors at pressure ratios close to unity. However, the flow on the compressor side is almost steady and the efficiency measurements are stable and repeatable even for very low turbocharger speeds.

4.2.2 Experimental Results

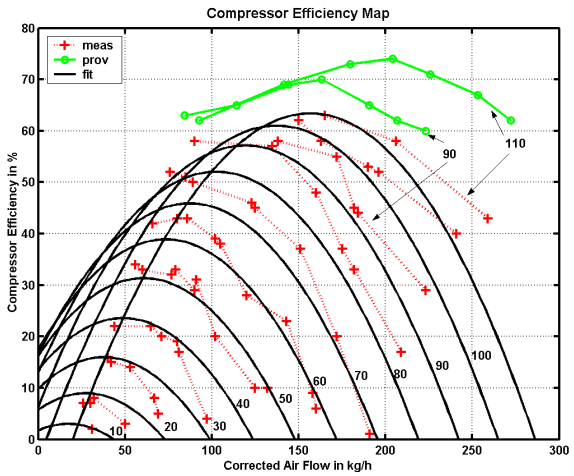

Figure 3: Compressor efficiency map: Measured, provided, and fitted data for different turbocharger speeds. The turbocharger speed labels are in krpm. Note that the provided and measured data are not directly comparable as discussed in Section 4.1.1. The provided data are plotted for qualitative comparison only.

Figure 3 shows the experimental compressor efficiency data plotted versus the corrected compressor flow. The efficiency decreases significantly with decreasing corrected turbocharger speed. This is due to the heat transfer effect mentioned in Section 1 (this will become apparent from the turbine efficiency maps in Section 4.4). At low airflows observed at low turbocharger

speeds, the turbocharger housing acts as a quite effective heat exchanger, which transfers heat from the exhaust to the intake manifold, thereby rising the post compressor pressure. This results in an artificially low isentropic efficiency in (19), which does not reflect the pure aerodynamic efficiency anymore.

4.2.3 Discussion

The compressor efficiency is used in the mean-value model for the calculation of the intake manifold temperature and the compressor power. With respect to the temperature, the artificially low (pseudo-) efficiency is actually needed to predict the correct temperature; otherwise it would be underestimated. Concerning the turbocharger speed calculation via the power balance (1), it will result in the correct values if the heat transfer effect is also considered on the turbine side, as will be done in Section 4.4.2.

The mismatch between the measured and provided efficiency curves at 90,000 and 110,000 rpm is significant, but again due to the assumption of ambient conditions at the compressor inlet. As for the compressor flow, using constant ambient conditions upstream of the compressor in the mean-value model implies that the measured map should be parameterized, thereby avoiding to model the pressure drop and temperature rise separately. Although the provided data are therefore not directly comparable to the measurements, they are plotted for a qualitative comparison. Again, using the measured upstream conditions results in a good agreement with the provided data.

4.3 TURBINE FLOW

4.3.1 Measurement

While the pressure ratio across the turbine can be measured with the appropriate sensors directly, the turbine flow needs to be inferred from the mass flow into the engine measured with the MAF sensor. In steady-state, even with EGR, the turbine mass flow equals compressor mass flow plus fuel flow (‘what goes into the engine must come out’).

4.3.2 Experimental Results

Figure 4 depicts the experimental data obtained for six different VGT positions. For increasing VGT position, the turbine restricts the flow more and more, resulting in less flow at the same pressure ratio. The turbine flow map turns out to be almost independent of the turbocharger speed and therefore three- rather than four-dimensional.

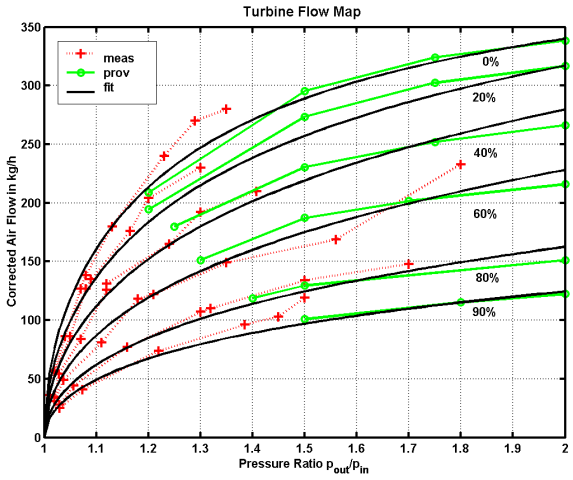

Figure 4: Turbine flow map: Measured, provided and fitted data for different VGT positions (0 % is fully open).

4.3.3 Discussion

The measured data extend the provided maps smoothly to pressure ratios down to unity. However, there are discrepancies at some operating points. As mentioned in Section 4.1.1, these could be due to measurement errors of the MAF sensor. Therefore, the more accurately obtained provided turbine flow map has been used for parameterization at higher pressure ratios, while the measured data constitute the basis for the extension to pressure ratios close to unity.

4.4 TURBINE EFFICIENCY

4.4.1 Measurement

As for the compressor efficiency, the turbine efficiency cannot be measured directly, but has to be calculated from temperature and pressure data. Rearranging (7) results in

$$\eta_t = \frac{1 - \frac{T_t}{T_x}}{1 - \left(\frac{p_t}{p_x}\right)^{\frac{\gamma-1}{\gamma}}} \tag{20}$$

which becomes sensitive to measurement errors at pressure and temperature ratios close to one. As opposed to the compressor side, the pulsating flow in the exhaust renders the pressure ratio measurement very fluctuating. Moreover, a closed-coupled oxidation catalyst with its high thermal inertia affects the post turbine temperature. Exothermal reactions in the catalyst can raise this temperature above the pre turbine temperature, leading to negative efficiencies. Besides, it

is impractical to wait for the temperatures to assume equilibrium at each new operating point, especially when going from high to low loads.

These technical problems can be overcome as follows: According to (1), the power balance between turbine and compressor is in equilibrium once the turbocharger speed (as well as the pressure ratio and temperatures) have assumed their steady-state values at a given operating point. Hence, setting (1) equal to zero and plugging in the expressions for the compressor and turbine power (6) and (8), respectively, yields after rearranging

$$\eta_t \eta_c = \frac{T_a}{T_x} \cdot \frac{\left(\frac{p_c}{p_a}\right)^{\frac{\gamma-1}{\gamma}} - 1}{1 - \left(\frac{p_t}{p_x}\right)^{\frac{\gamma-1}{\gamma}}} \cdot \frac{W_{ci}}{W_{xt}} \qquad (21)$$

which is now independent of the post turbine temperature at the expense of the dependence on compressor efficiency, pressure, and temperature. However, these variables can be measured reliably. Despite the pulsating flow, steady and repeatable values for the turbine efficiency could be obtained for turbine pressure ratios down to 1.03. The turbine flow is again simply the sum of the compressor and fuel flows.

4.4.2 Experimental Results

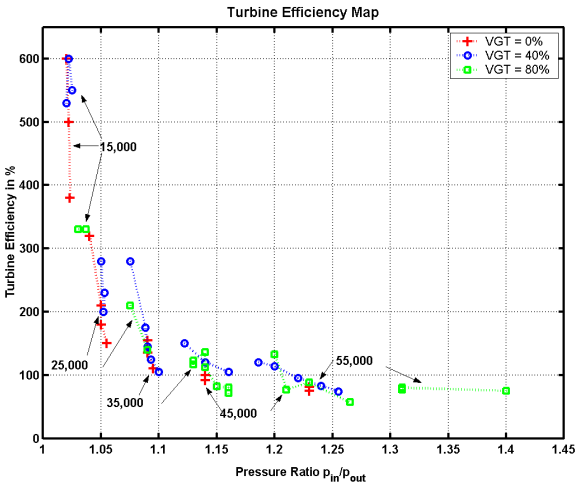

Figure 5: Turbine efficiency map: Measured data for different VGT positions (0 % is fully open) and turbocharger speeds.

In Figure 5, the turbine efficiency is plotted versus the turbine pressure ratio for three different VGT positions and corrected turbocharger speeds from 15,000 to 55,000 rpm. At pressure ratios below 1.2, the turbine efficiencies exceed 100 %, which is due to the effect of heat transfer. These values are calculated based on the compressor efficiency measurements according to (21), which in turn implies that those values are artificially low due to the heat transfer.

For different VGT positions, the speedlines cover a different range of pressure ratios, which is due to closing the vanes with increasing VGT position and thereby restricting the flow more. As mentioned in Section 4.4.1, no reliable values could be measured for pressure ratios below 1.03.

4.4.3 Discussion

At higher turbocharger speeds, the effect of the heat transfer becomes less significant. Ideally, the measured data would converge to the provided maps, which are available for corrected turbocharger speeds larger than 50,000 rpm and pressure ratios larger than 1.3. The provided turbine efficiency values lie in the range between 50 % and 65 % depending on the turbocharger speed and VGT position (Figure 6). Although they are not plotted in Figure 5 for reasons of clarity, the agreement to the measured values in this range is reasonable. This is especially true considering the observation in [8] that a loss of up to 30 % in turbine efficiency can be reached under the pulsating conditions in an engine as opposed to the steady-flow conditions under which the provided maps are obtained.

5 TURBOCHARGER PARAMETERIZATION

5.1 COMPRESSOR FLOW

For the compressor flow map, different parameterization methods have been developed and tested in the literature. A good overview can be found in [9], which especially investigates the extrapolation capabilities to lower turbocharger speeds. In this paper, the data for the whole low and medium load operating regime is available and a simple regression leading to a third-order polynomial in turbocharger speed and compressor flow has been found most straightforward with satisfying accuracy as can be seen in Figure 2, where the black lines denote the fitted curves. Additionally, the curve fit was validated in simulations with measured turbocharger speed as input which decouples the flow from the efficiency maps.

Due to the low slope of the compressor speed lines, it turned out to be beneficial to parameterize the pressure ratio across the turbine as function of the corrected flow and the turbocharger speed. However, this introduces an algebraic loop, which can be broken by using the momentum equation for the mass flow in the tube connecting the compressor outlet and the intake manifold

$$\dot{W}_{ci} = \frac{A}{l}(p_c - p_i) \qquad (22)$$

where *l* is the length of the tube and *A* its cross sectional area. Since the engine is equipped with the production type intercooler, this pipe is actually more than three meters long for packaging reasons. Thus, the dynamics are not fast enough to increase the stiffness of the model and thereby the simulation time significantly.

5.2 COMPRESSOR EFFICIENCY

As for the compressor flow, the efficiency map is parameterized using a regression leading to a third-order polynomial in turbocharger speed and compressor flow. The fitted curves are plotted in Figure 3 (black lines). The regression is reasonably good, especially in comparison to the uncertainty that is introduced by the sensitivity of the efficiency to slight temperature changes.

5.3 TURBINE FLOW

Due to the nature of the turbine flow, a physics-based parameterization is the obvious choice using the standard orifice flow equation (14), where the effective area is identified as a linear function of the VGT position and corrected linearly based on the pressure ratio. The correction improves the fit at low pressure ratios, which are emphasized in this paper.

5.4 TURBINE EFFICIENCY

The turbine efficiency map is the most difficult to parameterize. Firstly, this is due to the dependence of the efficiency on pressure ratio, turbocharger speed, and VGT position rendering the map four-dimensional. Secondly, the effect of heat transfer increases the range of the efficiencies leading to pseudo-efficiencies of more than 600 % at pressure ratios close to unity. Regressions have been found not to be suitable, mainly due to lack of data. The way forward suggested in this paper is to separate the aerodynamic efficiency and the efficiency added due to the heat transfer effect. The aerodynamic efficiency can then be modeled using a conventional approach based on the so-called blade speed ratio (Section 5.4.1), while the efficiency due to heat transfer is parameterized based on a heat exchanger equation with flow-dependent effectiveness (Section 5.4.2).

This approach requires the separation of the two efficiencies, which can be done conveniently by splitting up the post turbine temperature into two terms

$$T_t = T_{t,aero} - T_{t,heat} \tag{23}$$

This reflects the fact that the measured temperature T_t is equal to the one obtained by using the purely aerodynamic efficiency $T_{t,aero}$ in (7) minus the temperature drop due to the heat transfer via the turbocharger housing $T_{t,heat}$. Applying (23) to (20) results in the separation of the pseudo-efficiency into the aerodynamic efficiency and the efficiency due to heat transfer

$$\eta_{t,pseudo} = \eta_{t,aero} + \frac{\frac{T_{t,heat}}{T_x}}{1-\left(\frac{p_t}{p_x}\right)^{\frac{\gamma-1}{\gamma}}} = \eta_{t,aero} + \eta_{t,heat} \tag{24}$$

If no heat loss occurs, the pseudo-efficiency is equal to the aerodynamic efficiency. Even for very small losses, the efficiency due to heat transfer increases significantly with decreasing pressure ratios due to their appearance in the denominator. This effect is shown in Figure 6, where $\eta_{t,heat}$ is plotted versus the pressure ratio for $T_{t,heat}$ being equal to 1 % of T_x. Comparing Figure 6 to Figure 5 indicates that this might be a reasonable way to parameterize the turbine efficiency.

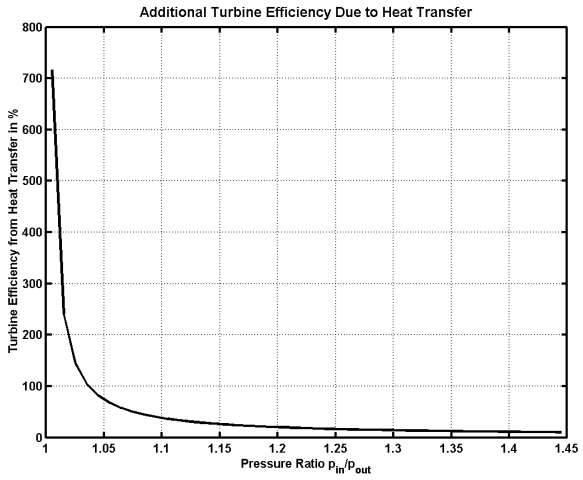

Figure 6: Turbine efficiency due to heat transfer as a function of the turbine pressure ratio for a 1 % loss in temperature.

5.4.1 Parameterization of the Aerodynamic Efficiency

At low turbocharger speeds, the measured efficiency inevitably includes the heat transfer effect. Therefore, the supplied data for higher speeds is parameterized and extrapolated to lower speeds. Potential extrapolation errors will then be compensated in the parameterization of the efficiency due to heat transfer.

The conventional approach to parameterize the turbine efficiency is based on the blade speed ratio defined as

$$c_u = \frac{\pi D N_t}{60\sqrt{2c_p T_x\left(1-\left(p_t/p_x\right)^{\frac{\gamma-1}{\gamma}}\right)}} \tag{25}$$

where *D* denotes the turbine blade diameter. Note that this transformation does not introduce new independent variables. Some of the supplied data are plotted in Figure 7, which also shows the curve fitting.

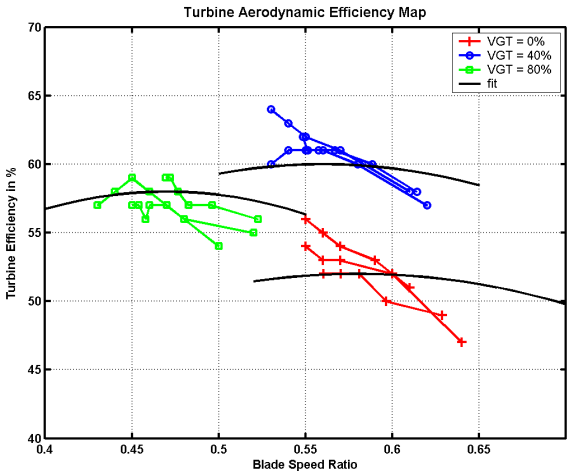

Figure 7: Turbine aerodynamic efficiency map: Provided and fitted data for different blade speed ratios and corrected turbocharger speeds (50, 60, and 70 krpm).

According to [4], the aerodynamic efficiency can be parameterized conveniently as a quadratic function in blade speed ratio

$$\eta_{t,aero} = \eta_{\max}\left(2\frac{c_u}{c_{u,opt}} - \left(\frac{c_u}{c_{u,opt}}\right)^2\right) \qquad (26)$$

where both η_{max} and $c_{u,opt}$ are regressed as polynomials in the VGT position only, without additional dependence on the turbocharger speed. This can be justified by the fact that the efficiency only changes little with turbocharger speed and lies well within the accuracy requirements for mean-value modeling. Moreover, the calculation of the efficiency from heat transfer is based on the measurements and the parameterized values for the aerodynamic efficiency, thereby implicitly compensating for the modeling errors.

5.4.2 Parameterization of the Efficiency from Heat Loss

From the parameterization (26), the aerodynamic efficiency can be calculated for a given operating point. Deducting this value from the measured (pseudo-) efficiency yields the efficiency added due to heat losses according to (24). Mapping these values directly is again a difficult task, since it is not obvious which independent variables should be chosen to avoid parameterizing a four-dimensional map (i.e. based on corrected turbocharger speed, pressure ratio, and VGT position). It is therefore suggested to employ the physics behind the heat transfer process, and hence to model the turbocharger as a heat exchanger. As will be seen later, this reduces the map to three dimensions and the data also confirm that this assumption is indeed reasonable.

The governing equation for a heat exchanger has already been introduced in (16). For the turbocharger, the upstream temperature is the exhaust manifold temperature, and the coolant temperature is chosen as the intake manifold temperature. From (16), the temperature drop due to heat transfer via the turbocharger housing can be derived as

$$T_{t,heat} = \eta_{VGT}\left(T_x - T_i\right) \qquad (27)$$

where η_{VGT} describes the cooling effectiveness of the turbocharger. For each engine operating point, the cooling effectiveness can be calculated by first deriving $T_{t,heat}$ from $\eta_{t,heat}$ in (24) and then applying (27). The effectiveness should decrease with increasing flow rate through the turbine and this is confirmed in Figure 8, where η_{VGT} is plotted versus the corrected turbine flow. Hence, the pseudo-efficiency converges to the aerodynamic efficiency at higher operating points. The dependence on the VGT position is also reasonable, since the flow velocity has to be higher to achieve the same flow rate through a more restricted turbine when the VGT is more closed. This implies that the effectiveness for the same flow rate should be less if the VGT is more closed which is confirmed in Figure 8.

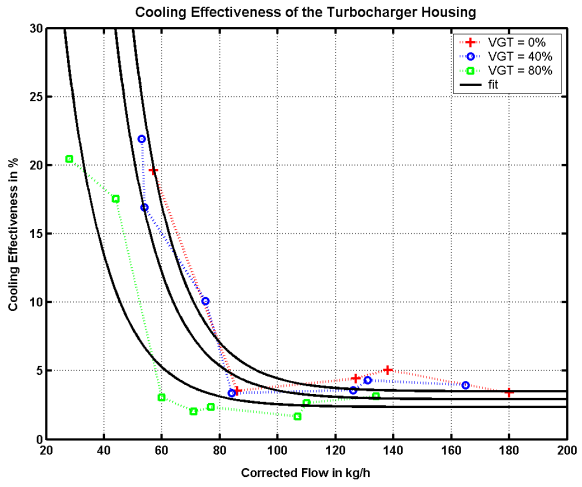

Figure 8: Cooling efficiency of the turbocharger for different corrected turbine flows and VGT positions.

Figure 8 also shows the curve fit, which has been chosen as

$$\eta_{VGT} = 30\exp\left(\frac{1}{15}\left(x - x_0\right)\right) + x_1 \qquad (28)$$

where x_0 is a quadratic and x_1 a linear function of the VGT position.

6 EXPERIMENTAL VALIDATION

In models for control, the steady-state accuracy is less important since any reasonable controller will take care of steady-state errors. It is rather the dynamic behavior of the plant especially at frequencies around the intended bandwidth of the closed-loop system, which is important. Therefore, the frequency response of the system is obtained in Section 6.2. This is done by applying sinusoidal inputs of different frequencies and amplitudes, which is also a good way of assessing the degree of nonlinearity of the system. In Section 6.3, data obtained from the New European Drive Cycle (NEDC) is used to assess the model accuracy in transients.

6.1 GENERAL REMARKS

In this paper, the focus of the modeling and validation is on the turbocharger, which is the crucial nonlinear part of the overall engine model. In order to avoid that errors in other submodels propagate to the VGT model, the crankshaft dynamics described in (9) are bypassed and the measured engine speed is used instead. Moreover, the EGR valve is kept shut to decouple the EGR from the VGT system. The compressor and turbine flow maps can be validated separately from the efficiency maps by feeding the measured turbocharger speed into the model. This has been done and the flow maps have been found to be satisfactory. The simulation results presented in the subsequent sections are all based on the simulated turbocharger speed.

6.2 FREQUENCY RESPONSE

Figure 9 shows the response of the system to a sinusoidal VGT position input at a constant speed-load operating point (1500 rpm, 85 Nm). Comparing the simulation (blue, dashed) and experimental data (red, solid) shows good agreement in the dynamic response, but steady-state offsets, especially in the compressor flow (upper right plot). However, this does not pose a problem for control design as mentioned above. Note that the turbocharger speed between 50,000 and 60,000 rpm lies well outside the range of the provided maps. The effect of heat transfer is significant, which can be seen in the lower right plot, where the turbine efficiency due to heat transfer is between 40 and 60 %, and the pseudo-efficiency exceeds 100%. Note that all signals are solely sinusoids of the same frequency indicating that the system behaves linearly with respect to the VGT position input at that operating point. Hence, the frequency response is obtained for that operating point in the following.

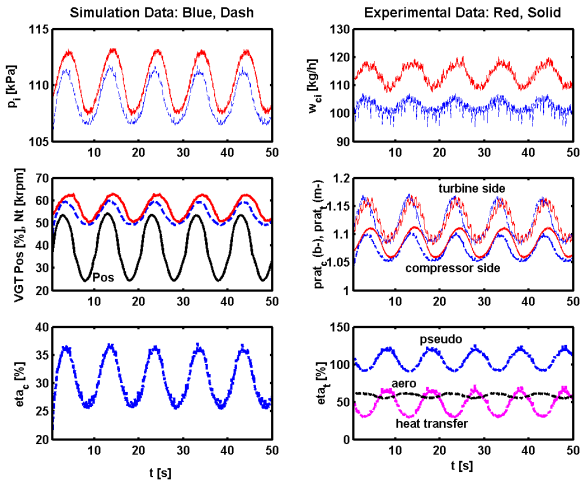

Figure 9: Engine response to a sinusoidal VGT position input at 1500 rpm, 85 Nm. Experimental data in red, solid lines, simulation data in blue, dashed lines; the other colors are labeled in the plots.

In engine applications, the VGT position is typically chosen to track a reference intake manifold air pressure (MAP or p_i) signal, which is optimized over the whole speed-load operating envelope of the engine. Hence, the frequency response of the system from VGT position to intake manifold pressure is obtained experimentally by applying sinusoids of different frequencies. Figure 10 shows the experimental frequency response in comparison to the one based on simulation results. For better comparison, the data points have been fitted with second-order transfer functions (simulation: blue, dashed line, experiment: red, solid line).

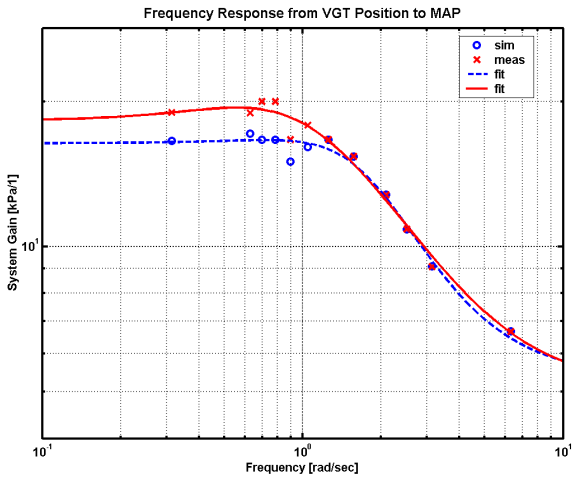

Figure 10: Experimental and simulated frequency response from VGT position to intake manifold pressure calculated from different sinusoidal excitations such as in Figure 9. The engine operating point is 1500 rpm, 85 Nm.

In this experiment, a constant amplitude sinusoidal duty cycle is commanded to the electronic vacuum regulator (EVRV), which results in sinusoidal VGT position excitations that are subsequently considered as the input to the system. However, due to the inability of tracking arbitrarily high frequencies, the amplitude of the VGT position will eventually become smaller. This does not make a difference for purely linear systems, where the system gain is constant. For the nonlinear system under investigation, the investigation of gain variations is part of further work.

Figure 10 shows that the low frequency gain is underestimated in the model, while the agreement in the medium and higher frequencies range is very good. As mentioned before, the difference in low frequency gain does not pose a problem for control design. The good agreement at higher frequencies is also due to the smaller amplitudes of the sinusoidal VGT position, which would not track larger excitations anymore. Therefore, potential gain nonlinearities are not excited as much as they are in the low frequency range.

6.3 DRIVE CYCLE DATA

In order to validate the model over a range of engine operating points, 50 seconds of the extra urban part of the New European Drive Cycle (NEDC) are chosen as transient excitation. The engine speed, fuel rate, and VGT position are used as input to the simulation model. A comparison of the experimental and simulation data is given in Figure 11. The overall agreement is quite good, but overshoots in the simulated turbocharger speed result in overshoots in the intake manifold pressure, and hence in the pressure ratio across the compressor. However, this can be improved by either increasing the turbocharger's inertia or by low-pass filtering the VGT position input.

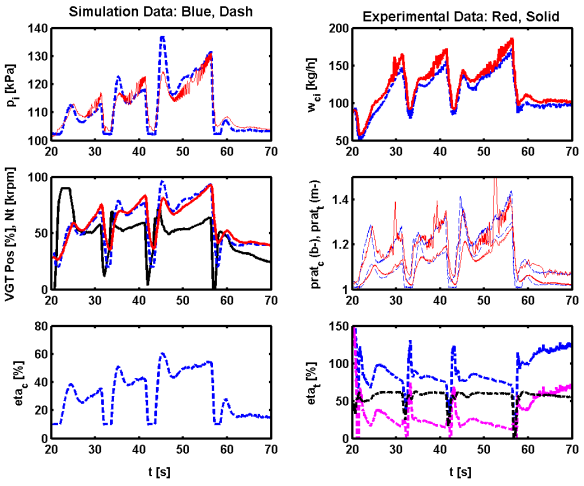

Figure 11: Experimental and simulation results for part of the New European Drive Cycle (NEDC). Experimental data in red, solid lines, simulation data in blue, dashed lines; the other colors are equivalent to Figure 9.

It could be argued that the over- and undershoots in the turbocharger speed are due to the fact that the effect of heat transfer on the efficiencies is modeled statically although it might be a rather slow process compared to the transients encountered in the NEDC. However, it is the aerodynamic efficiency, which determines the turbocharger speed on the engine. The heat transfer effect is only included in the model because it cannot be separated when inferring the turbocharger efficiencies based on temperature measurements and it is needed to give the correct post compressor and turbine temperatures. Hence, if the measured compressor and turbine efficiency maps, which include the effect of heat transfer, are to be used rather than the extrapolation of the aerodynamic efficiencies, the artificially low compressor efficiency will be compensated by the artificially high turbine efficiency, thereby canceling out the heat transfer effect when determining the turbocharger speed. Figure 11 shows that this works well for turbocharger speeds as low as 40,000 rpm. At even lower speeds, the pressure ratios across the compressor and turbine are close to unity resulting in a high sensitivity to modeling errors (cf. Figure 5). Therefore, a lower limit of 10 % for the compressor efficiency had to be chosen to avoid stalling of the turbocharger at very low pressure ratios in the simulation.

Note that the turbocharger speed between 30,000 to 90,000 rpm lies mostly well outside the range of the provided maps. The effect of heat transfer is significant, which can be seen in the compressor and turbine efficiency plots. The turbine pseudo-efficiency exceeds 100 % and the efficiency due to heat transfer (lower right plot, magenta line), which is added to the aerodynamic efficiency (black line), is significant. This indicates that the concept of including the heat transfer effect in order to use the experimentally obtained efficiency maps works well.

7 CONCLUSION

The following conclusions can be drawn from the work in this paper:

- Maps for the compressor and turbine flows and efficiencies have been obtained experimentally for low and medium turbocharger speeds. This operating region is typically excluded from maps provided by the supplier so that most models rely on extrapolation.
- Deriving the turbine efficiency from the compressor efficiency turned out to be a robust way to avoid the need for the post turbine temperature, which was difficult to measure due to a closed-coupled oxidation catalyst.
- The effect of the heat transfer from the turbine to the compressor side on the efficiency maps has been pointed out.

- A new way of parameterizing the turbine efficiency map including the effect of heat transfer has been suggested.
- Validation with engine data confirms the need to include the heat transfer effect to be able to predict the turbocharger speed at low speed-load operating points which are regularly encountered in emission drive cycles.

Although the measurements have only been obtained for one particular turbocharger on one particular engine, the authors feel that the same problems occur in other setups as well. Hence, the proposed way of including the heat transfer effect for low and medium turbocharger speeds would be beneficial for any engine model of this type.

ACKNOWLEDGMENTS

The first author acknowledges financial support in part by the European Commission through the program Training and Mobility of Researchers - Research Networks and through project System Identification (FMRX CT98 0206) and acknowledges contacts with the participants in the European Research Network System Identification (ERNSI). Additional financial and technical support from the Ford Motor Company is also gratefully acknowledged. All supplied turbocharger data are courtesy of Honeywell Garrett.

REFERENCES

1. M. Ammann, N. Fekete, A. Amstutz, L. Guzzella. Control-Oriented Modelling of a Turbocharged Common-Rail Diesel Engine, 3rd International Conference on Control and Diagnostics in Automotive Applications, Sestri Levante, Italy, 2001.
2. U. Christen, K. Vantine, N. Collings. Event-Based Mean-Value Modeling of DI Diesel Engines for Controller Design, *SAE*, Paper 2001-01-1242, 2001.
3. Z. Filipi, Y. Wang, D. Assanis. Effect of Variable Geometry Turbine (VGT) on Diesel Engine and Vehicle System Transient Response, *SAE*, Paper 2001-01-1247, 2001.
4. L. Guzzella, A. Amstutz. Control of Diesel Engines, *IEEE Control Systems Magazine*, vol. 18, no. 5, pp. 53 – 71, 1998.
5. J. Heywood. *Internal Combustion Engine Fundamentals*, McGraw-Hill, New York, 1998.
6. J. Jensen, A. Kristensen, S. Sorensen, N. Houbak, E. Hendricks. Mean Value Modeling of a Small Turbocharged Diesel Engine, *SAE*, Paper 910070, 1991.
7. M. Kao, J. Moskwa. Turbocharged Diesel Engine Modeling for Nonlinear Engine Control and State Estimation, *ASME Journal of Dynamic Systems, Measurement, and Control*, vol. 117, 1995.
8. J. Lujan, J. Galindo, J. Serrano. Efficiency Characterization of Centripetal Turbines under Pulsating Flow Conditions, *SAE*, Paper 2001-01-0272, 2001.
9. P. Moraal, I. Kolmanovsky. Turbocharger Modeling for Automotive Control Applications, *SAE*, Paper 1999-01-0908, 1999.
10. M. Mueller, E. Hendricks, S. Sorenson. Mean Value Modelling of Turbocharged Spark Ignition Engines, *SAE*, Paper 980784, 1998.
11. K. Vantine, U. Christen, K. Glover, N. Collings. Analysis of an Event-Based Diesel Engine Model for Control Purposes, *3rd IFAC Workshop on Advances in Automotive Control*, Karlsruhe, Germany, 2001.
12. Y. Yacoub, A. Chevalier. Rapid Prototyping with the Controller Area Network (CAN), *SAE*, Paper 2001-01-1224, 2001.

CONTACT

Merten Jung
University of Cambridge
Department of Engineering
Trumpington Street
Cambridge, CB2 1PZ
United Kingdom

Jung@tu-harburg.de

NOTATION

SUBSCRIPTS

a	ambient
c	compressor
e	engine (cylinders)
i	intake (manifold)
is	isentropic
r	recirculation (EGR)
t	turbine
x	exhaust (manifold)

Mass flows are denoted with two subscripts, indicating the source and sink. For instance, W_{ci} is the flow from the compressor into the intake manifold, i.e. MAF.

SYMBOLS

A	m^2	cross-sectional area
A_r	m^2	effective area of EGR valve
c_p	J/kg/K	specific heat ratio at constant pressure
c_v	J/kg/K	specific heat ratio at constant volume
c_u	-	blade speed ratio
D	m	turbine blade diameter
h	J/kg	specific enthalpy
$J_\bullet$	kg m^2	inertia
l	m	length
m	kg	mass in the manifold

N	rpm	engine speed
N_t	rpm	turbocharger speed
$N_t^{\sim}$	rpm	corrected turbocharger speed
P_c	W	power drawn by the compressor
P_t	W	power delivered by the turbine
$p_{\bullet}$	kPa	pressure
p_r	-	pressure ratio
R	J/kg/K	gas constant
t	s	time
$T_{\bullet}$	K	temperature
T_b	Nm	brake torque
T_l	Nm	load torque
$V_{\bullet}$	m3	volume
V_d	dm3	engine displacement
W_{ab}	kg/h	mass flow from a to b
x_r	-	normalized EGR valve lift
Φ	kg/h	normalized (corrected) mass flow
γ	-	specific heat ratio ($\gamma=c_p/c_v$)
$\eta_{\bullet}$	-	efficiency
η_{aero}	-	aerodynamic efficiency
η_{pseudo}	-	pseudo-efficiency
η_{heat}	-	efficiency due to heat transfer
$\eta_{h.e.}$	-	heat exchanger effectiveness
η_v	-	volumetric efficiency
η_{VGT}	-	cooling effectiveness of the VGT